ACS APPLIED MATERIALS & INTERFACES

Research Article

www.acsami.org

Bioinspired Multifunctional Hetero-Hierarchical Micro/Nanostructure Tetragonal Array with Self-Cleaning, Anticorrosion, and Concentrators for the SERS Detection

Qiao-Xin Zhang,[†] Yu-Xue Chen,[†] Zheng Guo,[‡] Hong-Lin Liu,[‡] Da-Peng Wang,[‡] and Xing-Jiu Huang*[,†,‡]

[†]School of Mechanical and Electronic Engineering, Wuhan University of Technology, 122 Luoshi Road, Wuhan, 430070, P. R. China

[‡]Research Center for Biomimetic Functional Materials and Sensing Devices, Institute of Intelligent Machines, Chinese Academy of Sciences, Hefei, 230031, P. R. China

Supporting Information

ABSTRACT: Heterohierarchical micro/nanostructure tetragonal array consisted of engineering materials of microprotrusion-like Cu and secondary nanostructured dendrite Ag have been fabricated via a primary cell-induced deposition and a facile galvanic displacement reaction combined with photolithography technique on Cu foil. Confined by the circle microwell tetragonal array of the photoresist template, regular microprotrusion-like Cu with the tunable size of diameter can be easily deposited on the surface of Cu foil. Then, the secondary dendritic Ag nanostructures in situ grow on the surface of microprotrusion via a galvanic displacement reaction, leading to the formation of heterohierarchical micro/nanostructure tetragonal array, which is similar to the surface microstructure of the lotus leaf. Inspired by this novel surface structure of imitating lotus leaf, its wettability has been systematically investigated. The results indicate that the fabricated heterohierarchical micro/nanostructure regular array after the surface fluoration presents a remarkable superhydrophobic performance. Initiated from its superhydrophobicity, an excellent self-cleaning property has also been demonstrated. In addition, the durability of the superhydrophobic surfaces is examined in the wide pH range of corrosive liquids. Notably, the fabricated superhydrophobic surface can be potentially used as concentrators, which presents a great perspective in the field of analysis through employing the SERS detection as an example.

KEYWORDS: *heterohierarchical, superhydrophobicity, micro/nanostructure, self-cleaning, anticorrosion*

INTRODUCTION

In nature and our daily life, the surface wettability is an important and universal phenomenon. Especially inspired by the self-cleaning of "Lotus effect", the wetting behaviors of superhydrophobic surfaces with a high water contact angle (>150°) and low contact angle hysteresis (<5°) have been received great attentions in the past several decades.[1,2] Superhydrophobicity, as a classical physical phenomenon, is still a hot research topic till now because of its perspective applications in various fields including self-cleaning, oil−water separation, drag reduction, and microfluidic devices and so on.[3−7]

As is well-known, the superhydrophobicity of the lotus leaves mainly come from the hierarchical micro/nanostructures instead of only effect of the epicuticular waxes.[8] Consequently, to realize superhydrophobic surface analogous to the "Lotus effect", it should be with a proper topographical structure besides the low surface energy.[9,10] Initiated from this view, great efforts have been focused on constructing multiscale roughness structure surface through various physical and chemical approaches,[11] especially for the fabrication of various hierarchical micro/nanostructures.[12−19] For example, Babak et al. have fabricated a superhydrophobic hierarchical silicon surface with contact angle of 160° and a sliding angle of less than 1° through electrochemical surface modification.[20] Lee et al. have also fabricated biomimetic superhydrophobic surfaces on a regular hierarchical polymer substrate by heat- and pressure-driven imprinting methods using patterned AAOs as replication templates.[19] In our previous research, we also constructed ZnO/CuO heterohierarchical nanotrees array with self-cleaning properties.[21] Recently, metal, as important and irreplaceable engineered materials, have also been involved to the construction of the superhydrophobic surfaces, which will further widen their applications.[17,22−24] For example, via an electrodeposition method, hierarchical dendritic gold microstructures show a good superhydrophobic property with anticorrosion after a chemical modification with 1H,1H,2H,2H-perfluorodecanethiol.[25] Superhydrophobic stainless steel surfaces have also been created by invoking hydrofluoric acid etching.[26] A hierarchical copper structure combining micro- and nanogaps/pores was built up on copper substrate by etching and electrodeposition, which realized the

Received: July 1, 2013
Accepted: September 30, 2013
Published: September 30, 2013

wettability cycling between superhydrophobicity and superhydrophilicity.[27] Furthermore, by dislocation-selective chemical etching superhydrophobic surfaces on Al, Cu, and Zn substrates have also been reported.[28] Besides pure metals, some alloys can also be employed to fabricate the superhydrophobic surfaces.[29,30] Although various superhydrophobic surfaces with hierarchical structures have been constructed from polymers to metals, most of them are random and irregular, which limits the further specific applications.[31,32] Additionally, some of the fabricated processes are complex, time-consuming, and so on. Restricted by the aforementioned disadvantage, it is still desirable and necessary to develop simple approaches to fabricate a regular micro/nanostructure array surface with superhydrophobic performances.

Amount of previous researches have demonstrated that MEMS techniques as efficient methods have often been employed to fabricate regular patterns on various substrates.[33,34] For example, Chen et al. have prepared superhydrophobic surfaces of hierarchical structure of hybrid from nanoparticles and regular pillarlike pattern using an embossing method.[35] On the basis of geometric replica, a hierarchical roughness of PDMS surfaces with superhydrophobicity has been fabricated combining with the plasma treatment.[36] Although this approach has been widely applied to fabricate various patterns on many substrates, few reports have involved the construction of regular engineering materials, such as metals micro/nanostructure array with superhydrophobic performances.

Herein, regular heterohierarchical micro/nanostructure array composed of engineering materials of microprotrusion-like Cu and dendrite Ag has been first fabricated on Cu foils by combining photolithography techniques with primary cell-induced deposition and galvanic replacement methods. The whole preparation process is described in Scheme 1. First, microprotrusion-like Cu array is prepared via a primary cell-induced deposition on the surface of Cu foil with the circle microwell patterned array of the photoresist, which is fabricated by a photolithography approach. Then, directly immersing the foil with the patterned array into $AgNO_3$ solution, all protrusion microstructures are uniformly covered with in situ growing dendritic Ag nanostructures via a galvanic displacement reaction, leading to the formation of heterohierarchal micro/nanostructure array analogous to the surface microstructure of the lotus leaf. During the above two steps, solution concentration and reaction time are further optimized. Inspired by this novel surface structure of imitating lotus leaf, the wettability of regular heterohierarchical array surface has been investigated. Moreover, self-cleaning effect of their surface has also been explored. Additionally, the fabricated surface used as another function of concentrators has also been demonstrated and further applied for the SERS determination.

Scheme 1. Schematic Process of the Fabrication of Bioinspired Multifunctional Hetero-Hierarchical Micro/Nanostructure Tetragonal Array[a]

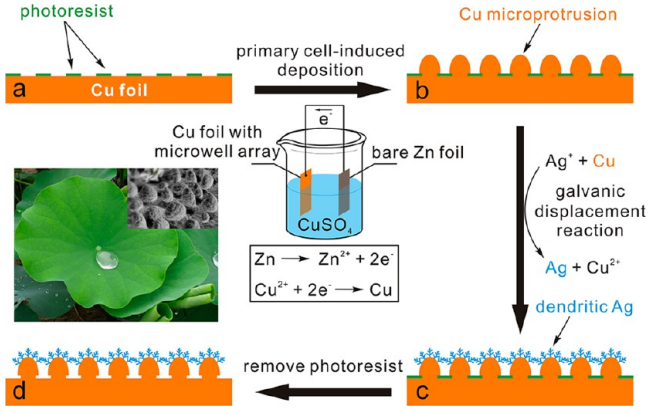

[a](a) Regular microwell array on Cu foil with the photoresist template after spin coating and exposure with UV; (b) electrodeposition of microprotrusion-like Cu via a cell-induced reaction; (c) in situ growth of secondary nanostructure dendrite Ag on the microprotrusion through a galvanic displacement reaction; (d) Lotus-like micro/nanostructures regular array after removing photoresist.

EXPERIMENTAL SECTION

Materials. Commercially available Cu and Zn foils (99.9% purity) were obtained from Sino pharm Chemical Reagent Ltd. Co. Other reagents and solvents, which were purchased from Shanghai Chemical Reagent Ltd. Co., are analytical grade and used as received without further purification.

Preparation of Microwell Tetragonal Array Pattern. Cu foils (Φ = 40 mm) were first immersed in the diluted hydrochloric acid solution to remove the oxide/hydroxide layer of their surfaces, and cleaned with acetone, alcohol and deionized water via an ultrasonication for 10 min to remove organic pollutants respectively. After dried with high purity following N_2, it is covered by a positive photoresist layer with a thickness of ~2 μm via a spin-coating approach. Following by the exposure of UV light with a photomask, circle-shaped microwell tetragonal array was formed by the photoresist on the Cu foil. The diameter of microwell was 8 μm, and the separated distance between adjacent microwells was also 8 μm.

Deposition of Heterohierarchical Micro/nanostructure Regular Array. A Cu foil (10 mm × 15 mm) fabricated with a regular microwell pattern and a bare Zn foil (10 mm × 15 mm) was employed as a cathode and an anode, respectively. After connected by a conducting wire, two foils with 20 mm of the separated distance were immersed into an aqueous solution of $CuSO_4$ with different concentrations varied from 0.1 to 0.5 M. After a certain reaction time, microprotrusion-like Cu array is formed on the Cu foil. It should be noted that the back side of Cu foil must be sealed by the insulating glue before the deposition. Afterward, the cleaned Cu foil with microprotrusion structures was dipped into 20 mM $AgNO_3$ solution. Then the galvanic reaction between Cu and Ag^+ rapidly happened, leading to the formation of dendrite Ag nanostructures. After being washed with acetone to completely remove the photoresist and the insulating glue, heterohierarchical micro/nanostructure regular array was finally obtained on the Cu foil.

Characterization. The surface morphologies and composition of as-fabricated samples were investigated by an Environmental Scanning Electron Microscopy (FESEM, FEI Quanta 200 FEG) equipped with an attached EDX system. The measurement of the contact angles of sessile drops were performed on an OCA20 system from Dataphysics GmbH, Germany, which was equipped with an high light transmitting capacity CCD camera and SCA 20 software. Prior to the measurements, the samples were chemically modified with 2 μL of ethanol solution of 20 mM 1H,1H,2H,2H-perfluorodecyltrichlorosilane (Alfa Aesar, USA) dropping on their surface for 2 h, inducing a layer of perfluorosilane. The 5 μL of water droplets was employed to measure the static contact angle. Each contact angle was measured repeatedly ten times at the different places on the samples and statistics value was recorded. SERS measurements were carried out with a confocal microprobe Raman system (LabRam HR800) using a laser of 632.85 nm and an objective lens (50×, Numerical Aperturec (NA) = 0.5) to reduce instrumental noise. The laser power was approximately 0.2 mW. Samples for SERS were prepared by casting the 10 μL of solution containing the analyte of crystal violet (CV, 1 μM) and Au nanoparticles (1×10^{11} particles/mL) on the fabricated superhydrophobic surface.

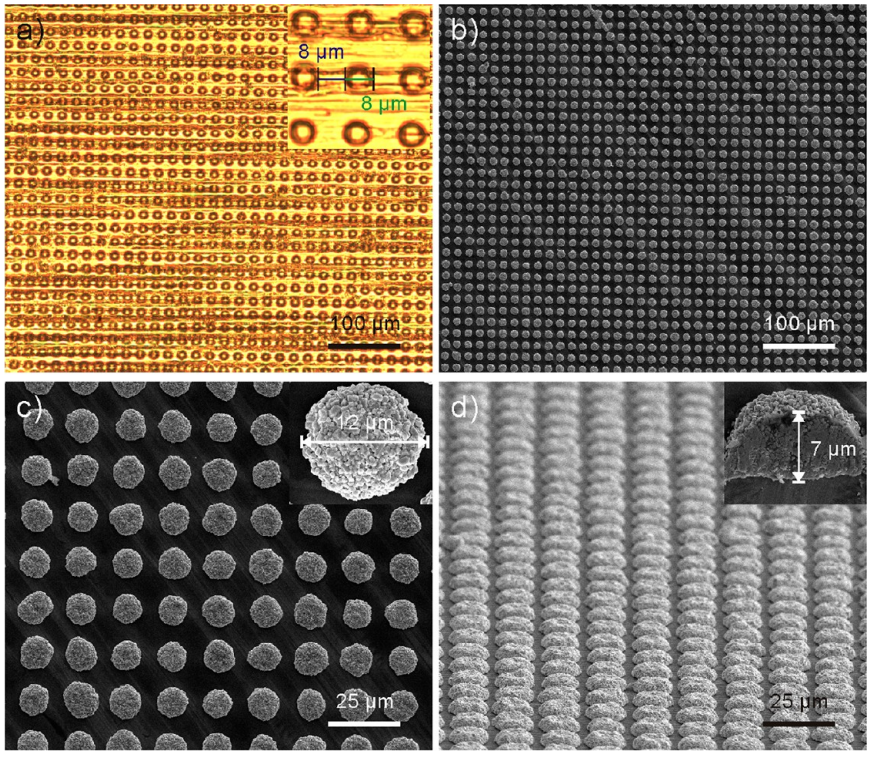

Figure 1. (a) Optical image of the fabricated microwell array on the Cu foil, the inset corresponding to the magnified image; (b) low-magnification SEM image of the morphology deposited in 0.2 M $CuSO_4$ solution for about 5 min; (c) high-magnification SEM image; (d) SEM image of the side view at 65°. The insets of c and d correspond to the top and side view of individual protrusion-like microstructure, respectively.

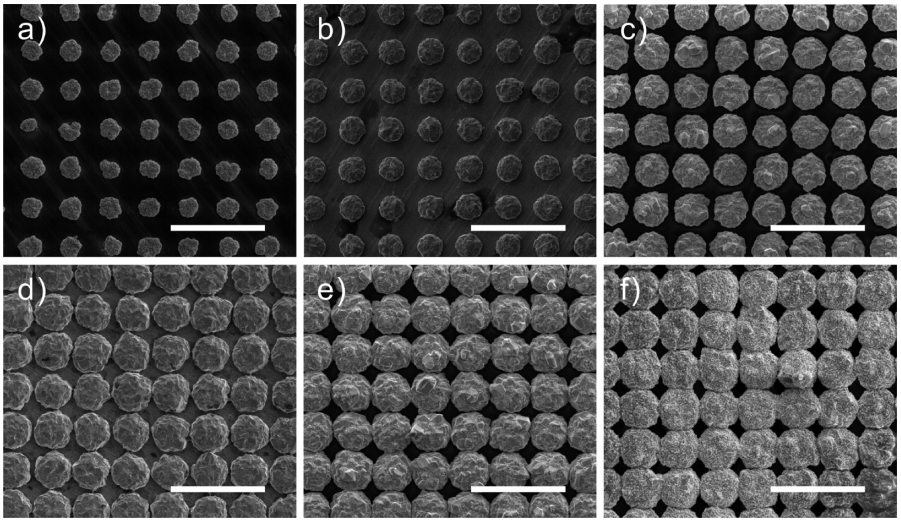

Figure 2. Morphology evolution of microprotrusion on the Cu foil with different deposition time in 0.2 M $CuSO_4$ solution: (a) 2, (b) 4, (c) 6, (d) 8, (e) 10, and (f) 12 min. Scale bar: 40 μm.

RESULTS AND DISCUSSION

As shown in Figure 1a, circle-shaped microwell tetragonal array is formed with the photoresist on the surface of Cu foil by illumination with UV light with a designed pattern mask. From the magnified optical image presented in the inset of Figure 1a, it could be found that the diameter of microwell is about 8 μm, with the separated distance of 8 μm, which is in good agreement with the pattern of the designed mask. When the Cu foil with as-fabricated pattern linked with a bare Zn foil is simultaneously immersed into the solution of $CuSO_4$ (0.2 M), a primary cell-induced deposition immediately happened. Then microprotrusion-like Cu is formed at the fabricated microwell. Figure 1b is a typical SEM image of microprotrusion structure array on the surface after depositing for 5 min. Evidently, the deposited microprotrusion array is very regular with a large scale. From the magnified SEM image shown in Figure 1c, it can be easily observed that they are almost uniform in the size of their diameter. On the basis of individual microprotrusion shown in the inset of Figure 1c, it can be seen that its diameter is about 12 μm and it is composed of amount of shaped Cu nanoparticles. Notably, the effect of space-confined deposition is clearly demonstrated.[37] The thin layer consisted of

photoresist is employed as an insulator to confine the reaction at the microwell and avoid the deposition of Cu at other places. Figure 1d is the SEM image of side view with 65°. Obviously, the protrusion-like microstructure could be regarded as a semimicrosphere. This result can be concluded from the side view of individual one, which is presented the inset of Figure 1d. The height is estimated to be about 7 μm.

In the following, the effect of the deposition time has been further explored. Figure 2 exhibits SEM images of their top view corresponding to the different depositing time. Clearly, the diameter of microprotrusion gradually increases with the increment of the deposition time. At the same time, the separated distance between microprotrusions gradually decreases. During this process, the microprotrusions keep the same morphology. When it increases to 8 min, adjacent microprotrusions exactly contact, as shown in Figure 2d. Continuously increasing the deposition time, they will be much closer. After 12 min, the microprotrusion almost becomes a square shape from the initial circular one in Figure 2f.

The relationship between the deposition time and the diameter of microprotrusion is also shown in the black line in Figure 3. Undoubtedly the morphological evolution of

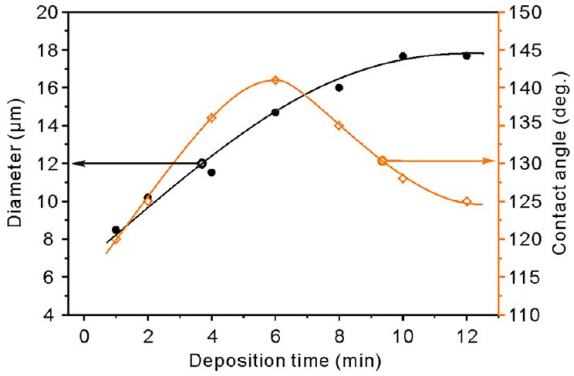

Figure 3. Effects of the deposition time in the 0.2 M $CuSO_4$ solution to the diameter of microprotrusion (black line) and the wettability of the fabricated surfaces after fluoration (yellow line).

protrusion-like microstructure is followed by a time-dependent relationship. Notably, at the deposition time of 8 min it is a critical point. The microprotrusion maximum diameter is about 16 μm due to the limitation of pattern. Actually, the concentration of $CuSO_4$ solution is also an important parameter for the deposition of Cu. Other concentrations besides 0.2 M have also been considered. The similar results have been obtained, as shown in Figure S1 (see the Supporting Information). When the deposition time is fixed, the diameter increases with the increase in $CuSO_4$ concentration.

Definitely, the wettability greatly depends on the surface roughness. To investigate the wettability of different deposited protrusion-like microstructure, we used the six samples shown in Figure 2. Before their fluoration, all of them are immersed into the acetone solution and washed several times to completely remove the photoresist and insulating glue. Afterward, they are rinsed with deionized water and dried at room temperature for further use. Via a surface fluoration, the static contact angles of six different morphologies have been measured. The results corresponding to the yellow line are shown in Figure 3. It clearly indicates that the contact angle first increases with the increment of the microprotrusion diameter. When the diameter increases to be about 14 μm at the deposition time of 6 min, the maximum contact angle about ~143° is obtained. With a larger diameter, it decreases gradually. Furthermore, this hydrophobic surface shows a large adhesive force, which can hold a spherical water droplet even it is turned upside down (More information seen in the following Figure 8). Although a high contact angle can be obtained through changing the diameter of the deposited microprotrusion, the superhydrophobicity is not still realized. It implies that the surface roughness is insufficient. Therefore, the roughness of the fabricated surface should be further improved.

Enlighten by the microstructure of lotus leaf, the wettability may be greatly improved through further fabricating a hierarchical nanostructure on the surface of microprotrusion. To demonstrate this idea, the sample deposited for 6 min has been employed, which corresponds to the maximum contact angle (~143°). According to the previous reports, dendritic Ag nanostructure can be easily formed on the Cu substrate in $AgNO_3$ solution via a galvanic replacement reaction.[38,39] Initiated from this principle, the selected sample follows the same reaction. With immersing it into $AgNO_3$ solution, the space-confined galvanic replacement reaction also happens at the exposed microprotrusion-like Cu. Then dendrite Ag in situ grows on the surface of the microprotrusion, leading to the formation of heterohierarchical micro/nanostructure. This result is strongly evidenced by a typical SEM image presented in Figure 4a. SEM phase mapping clearly reveals that Ag nanostructures uniformly covered on the microprotrusion-like Cu. As can be seen in Figure 4c, the shape of Ag element mapping fits well with the branched morphology for every protrusion in the selected area shown in Figure 4a. For Cu element, its distribution shown in Figure 4b cannot clearly follow the selected area owing to the interference of Cu foil. The elemental composition was further analyzed by EDX analysis, as described in Figure 4d. The strong peaks of Cu and Ag come from microprotrusion-like Cu and dendritic Ag. Any other element cannot be observed except for C element, which is from the photoresist.

Similar with the deposition of protrusion-like Cu, the growth of dendritic Ag also greatly depends on the reaction time, which is verified in Figure 5. Figure 5a–f shows SEM images of the morphology evolution for heterohierarchical micro/nanostructure array with the reaction time of 10, 30, 50, 70, 90, and 100 s, respectively. According to the reported literature,[40] the formation mechanism of the dendritic Ag nanostructure can be explained as a process of initial reduction, nucleation, adsorption, growth, branching and growth on the surface of the protrusion-like Cu. With the Cu foil exposed with the protrusion-like Cu dipped into $AgNO_3$ solution, the galvanic replacement reaction immediately happens. After 10 s of the reaction time, it could be found that Ag buds are formed on the surface of microprotrusion in Figure 5a. With the increasing reaction time, the dimension of dendritic Ag nanostructure also increases. Figure 5b shows the morphology of the surface deposited for 30 s. The growing nanostructure becomes bigger than that shown in Figure 5a. After deposition for 50 s, well-defined dendritic Ag nanostructures wrap tightly on the protrusion-like Cu and arranged along stems with symmetrical side branches and leaves, which is clearly observed in images c and d in Figure 5. Obviously, the regular heterohierarchical array is formed on the Cu foil, which is similar with the micro/nanostructure of lotus leaf. Further extension of the reaction time, Ag dendrite constantly increases and completely covers the substrate to form a film, which is demonstrated in Figure 5e

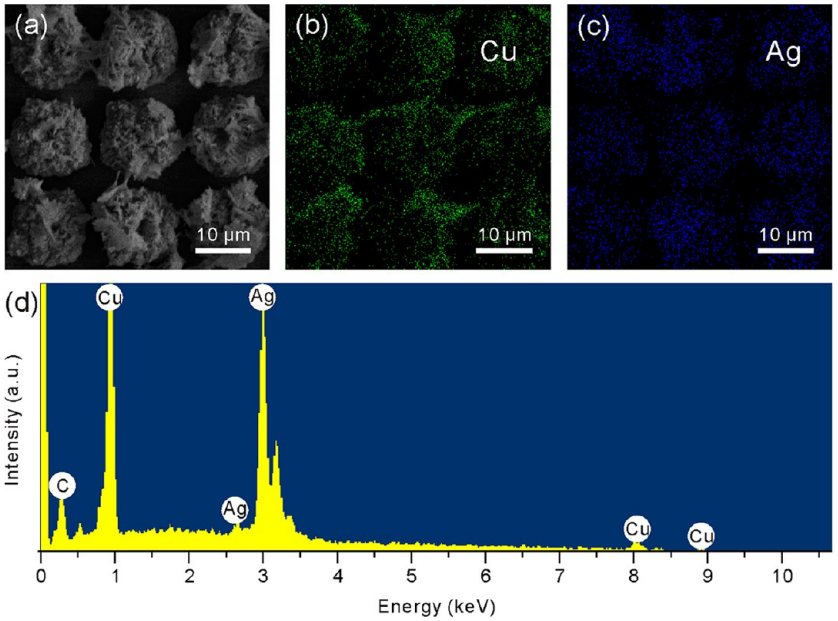

Figure 4. Component analysis of heterohierarchical micro/nanostructure tetragonal array consisted of microprotrusion-like Cu and nanodendrite Ag: (a) A typical SEM image, (b, c) Cu and Ag elemental mapping recorded from the same area to SEM image shown in image a, respectively. (d) Spectrum of EDX.

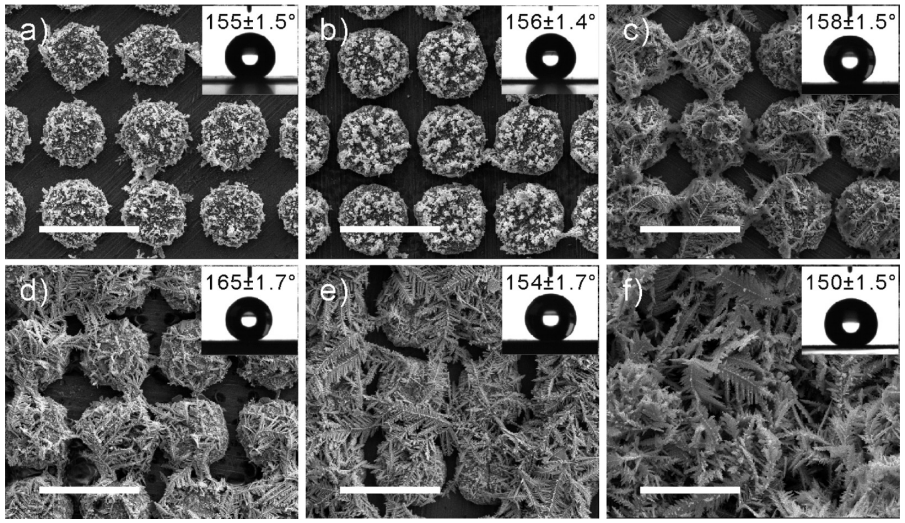

Figure 5. Morphology evolution of secondary nanostructure dendritic Ag on the surface of microprotrusion-like Cu with the galvanic displacement reaction time in the 20m M $AgNO_3$ solution: (a–f) 10, 30, 50, 70, 90, and 100 s, respectively. Static contact angles are shown in the insets of the corresponding samples. Scale bar: 20 μm.

and f. The wettability of the above prepared samples has been further explored. After the surface fluoration, they present a good superhydrophobic property that all of their static contact angles are above 150°. With the growth of Ag buds (Figure 5a) to Ag dendrites (Figure 5d), the static contact angle gradually increases from 155 ± 1.5° to 165 ± 1.7°, as shown in the inset of Figure 5a and Figure 5d, respectively. However, continuously prolonging the reaction time to 90 and 100s, Ag dendrites turn to be more compact, leading to the decrease of their contact angles down to 154 ± 1.7° and 150.5 ± 1.5° in images e and f in Figure 5. Obviously, through controlling the growth of Ag dendrites on the surface of microprotrusion-like Cu, the wettability can be manipulated from normal hydrophobicity to superhydrophobicity. Furthermore, the same process is also performed on the Cu foil uncovered with photoresist pattern. The morphologies of the deposited Cu and its further displacement by Ag ions are presented in Figure S2a and S2b, respectively (see the Supporting Information). Clearly, a thin and roughness Cu film without regular microprotrusions is formed on Cu foil without photoresist pattern via a primary cell-induced deposition. After its surface fluoration, the static contact angle shown in the inset of Figure S2a in the Supporting Information is about 128°, which is less than that of the regular Cu microprotrusion structure array. Through the further displacement reaction, random Ag dendritic nanostructure shown in Figure S2b in the Supporting Information is obtained, which is different from the regular heterohierarchical micro/nanostructure array using Cu foil with photoresist pattern. Its static contact angle is about 159° less than 165° of the regular heterohierarchical micro/nanostructure array.

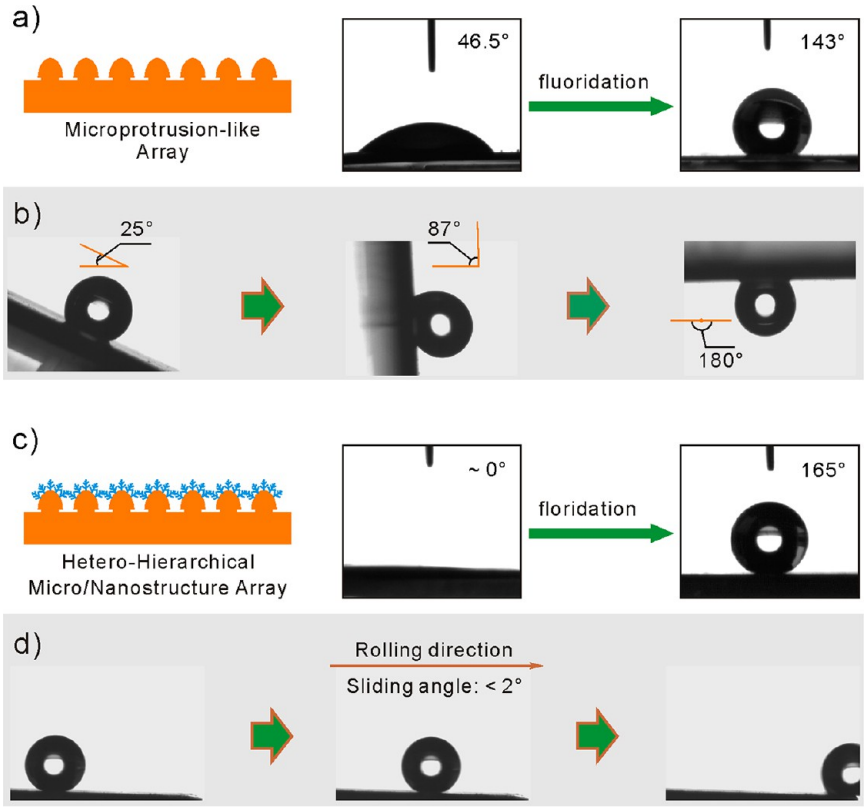

Figure 6. (a) Change of static contact angles for the surface with microprotrusion structure corresponding to the sample shown in Figure 2c before and after fluoridation, (b) shapes of the water droplet (5 μL) on the fluoridated surface with microprotrusion structures at tilt angles of 25, 87, and 180°; (c) change of static contact angles for the surface with heterohierarchical micro/nanostructure corresponding to the sample shown in Figure 5d before and after fluoridation; (d) snaps of the rolling water droplet at the sliding angle less than 2°.

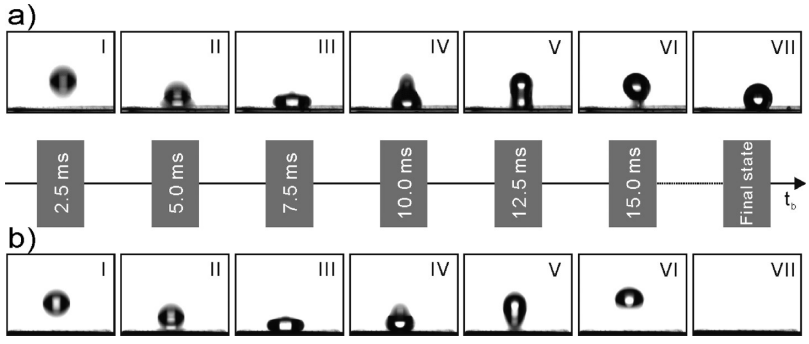

Figure 7. Snapshots of water droplet impacting the fabricated surfaces: (a) microprotrusion structure corresponding to the sample shown in Figure 2c and (b) micro/nanohierarchical array corresponding to the sample shown in Figure 5d.

Consequently, it can be concluded that the binary hierarchical micro/nanostructure can effectively improve the superhydrophobicity of surface.

To further illuminate the positive effect of superhydrophobicity arising from hierarchical micro/nanostructure, we have also investigated the sliding angle and contact angle hysteresis. For the protrusion-like microstructure, the static contact angle before and after the surface fluoration are 46.5 and 143°, respectively. Amazingly, with the formation of the hierarchical nanostructure, the water droplet will be rapidly and fully spread on its surface, presenting a superhydrophilicity. With introducing low free energy coatings, it turns to be superhydrophobicity with a high contact angle of 165°. This phenomenon proves that both hydrophobicity and hydrophilicity can be reinforced by roughness. For superhydrophobic surfaces, the sliding angle can give an index to the adhesive force of water on surfaces, which is defined as the critical angle when a water droplet begins to slide down an inclined plate. As illustrated in Figure 6b, the droplet basically keeps its original shape after it tilts to 25°. Then the droplet is deformed with the tilt angle increasing to 87°. Turning over the substrate, it is still tightly attached on the surface. However, the rolling angle of a droplet on the surface with hierarchical nanostructure after the fluoration is less than 2°, as shown in Figure 6d, meaning that the water droplet easily rolled off the surface. The difference of their sliding angles could be further demonstrated through their measurements of advancing and receding angle (more information seen in Figure S3 in the Supporting Information). On the basis of the above results, it is not difficult to conclude that the surface morphology structure has a great influence on

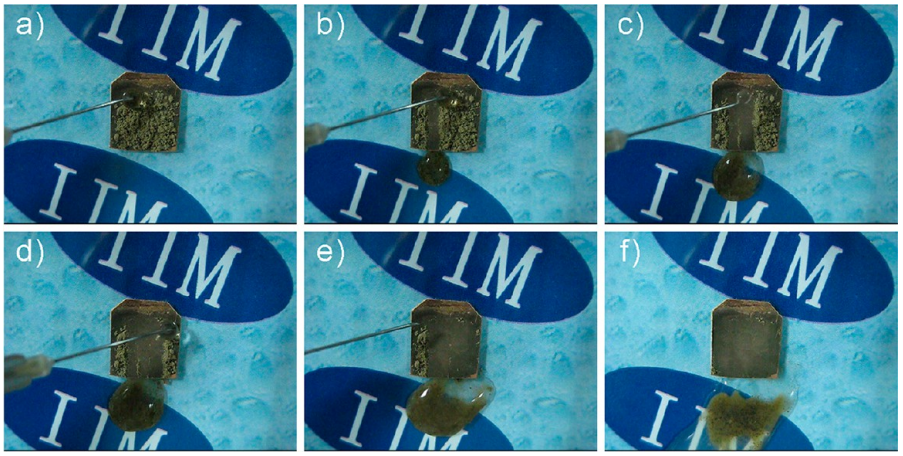

Figure 8. Self-cleaning performance of the fabricated superhydrophobic surface corresponding to the sample shown in Figure 5d with a layer of dust particles.

the adhesion force. Cassie and Baxter model is applied here to describe the contact angle of a superhydrophobic surface with low hysteresis. According to Cassie and Baxter model, there is an equation: $\cos\theta_r = f_1\cos\theta - f_2$, where f_1 and f_2 are the area fraction of the solid and air on the surface respectively ($f_1 + f_2 = 1$), that is: $\cos\theta_r = -1 + f_1(1 + \cos\theta)$, θ and θ_r are the intrinsic contact angle of the flat solid surface and the rough surface. In the case of the dual-roughness structure surfaces the experimental contact angles of the bare copper are treated as Young's contact angle, which is ~75°. The θ_r of the sample surface in Figure 6c is 165°. From the above equation, the value of f_2 is about 0.972, which means that about 97% of the rough surface area is covered by the air, and only 3% is in contact directly with water. The trapped air increases the interface between air and water, thus prevents the penetration of water droplets into the surface. This structure makes the water droplet suspend on the surface by the air trapped, resulting in the high surface contact angle. It indicates that the air trapped in the surface plays an important role in enhancing the surface superhydrophobicity.

In the following, the bouncing experiment is conducted by allowing a droplet of water to freely fall onto the fabricated surfaces. The whole process of a water droplet hitting the surfaces at the impact velocity of 43.8 cm s^{-1} and bouncing is shown in Figure 7. As shown in Figure 7a corresponding to the surface with microprotrusion-like Cu array, the droplet first deforms at the time of 5.0 ms and then fattens into a pancake. Subsequently, it retracts and tries to rebound off the surface. However, part of the droplet attaches to the substrate due to existing of the adhesion force and finally rests on the surface. On the contrary, it drops on the superhydrophobic surface with micro/nano heterohierarchical array rebounds upward elastically without leaving any residual traces on the surface. Compared with the former, the droplet keeps bouncing numerous times until it rolls off the surface. In order to further insight into its surface wettability, the relationship between the contact time of a bouncing drop and impacting velocity/drop radius was investigated (More information seen in Figure S4 in the Supporting Information). Similar results with our previous report have also been obtained.[21] This behavior is assumed to have a very significant effect on the self-cleaning property and the feasibility of its use as a friction-free surface.

To demonstrate the self-cleaning behaviors of the fabricated micro/nano heterohierarchical surface, a thick layer of dust particles as a representative example are uniformly spread on its surface, as described in Figure 8a. With a droplet of water added and rolled onto the surface, the covered dust particles can be easily removed from the surface along the rolling area of water droplets, which is clearly presented in Figure 8b. The same phenomenon is also followed by a series of water droplets. Their rolling traces without any remained dust particles can be clearly seen in Figure 8c–e. Finally, the dust particles on the surface are completely removed, as shown in Figure 8f. It indicates that the surface with heterohierarchical micro/nanostructure array is of great self-cleaning performance.

Additionally, the as-prepared fluoridated surface with regular heterohierarchical micro/nanostructure array presents superhydrophobic performance not only for pure water but also for corrosive water under both acidic and basic environment. The relationship between pH value and water contact angle of the superhydrophobic surface are depicted in Figure 9. Clearly there is no obvious fluctuation of static contact angles on the fabricated surface within experimental error when the pH value is varied from 1 to 14. The static contact angle almost keeps a constant value of about 165°, showing no effect of acid and base on the wettability of the surface, which is similar to previous reports.[41−44] To further demonstrate its anticorrosion

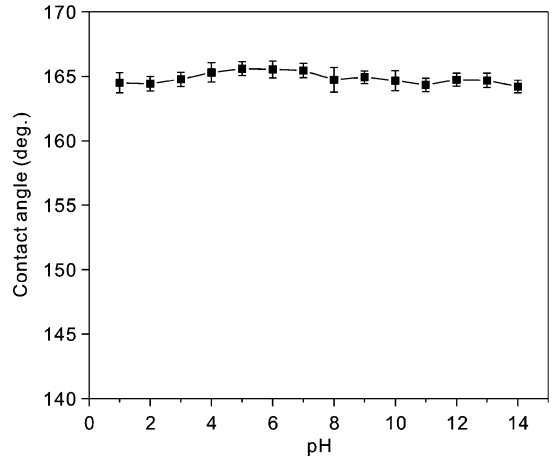

Figure 9. Relationship between the pH value and the water contact angle of as-prepared superhydrophobic surface corresponding to the sample shown in Figure 5d.

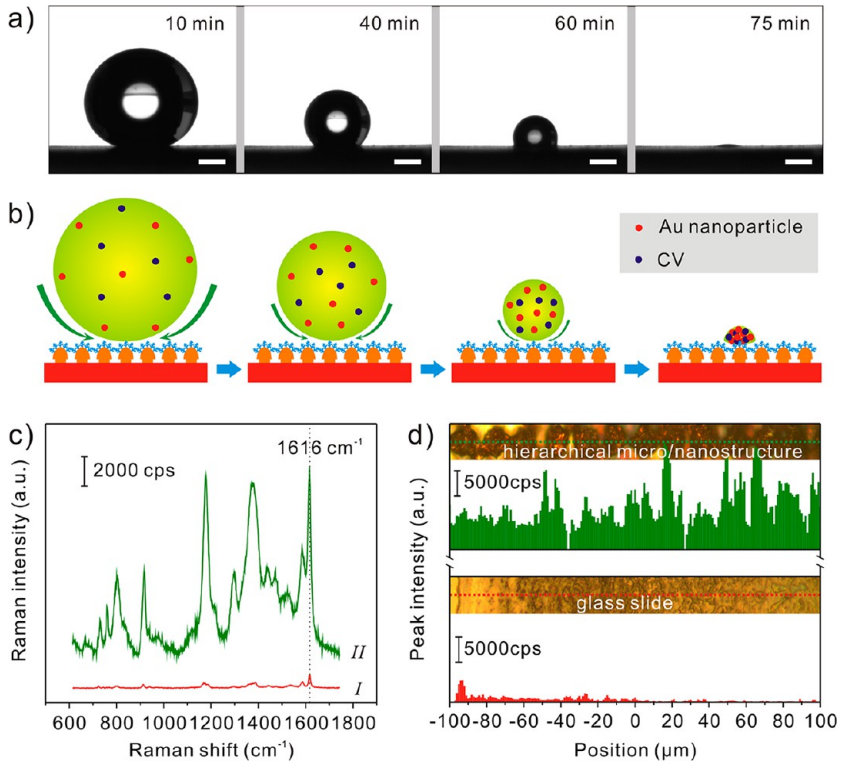

Figure 10. (a) Optical morphology evolution of the evaporation of a water droplet (10 μL) under ambient conditions, scale bar: 0.5 mm. (b) Schematic process of the evaporation a droplet solution containing Au nanoparticles and crystal violet (10 μL, 1 μM) on the fabricated superhydrophobic surface. (c) Raman spectra recorded on the hydrophilic glass slide (I, red curve) and the fabricated superhydrophobic surface (II, green curve). (d) Change of the peak intensity at1 616 cm^{-1} for the glass slide (bottom, along the scanning red line) and the fabricated surface with heterohierarchical micro/nanostructure regular array (top, along the scanning green line).

in the real application, we have further investigated the stability of the obtained superhydrophobic surface under strong acid solution, strong base solution, and 3.5 wt % NaCl aqueous solution, as shown in Figure S5 (see the Supporting Information). It can found that the static contact angles are fundamentally unchanged after immersing the fabricated surface into 3.5 wt % NaCl aqueous solutions with different time. Additionally, under strong base solution (pH 14) the same phenomena is observed, meaning that the fabricated superhydrophobic surface is with good stability under the above two solutions. However, when it is immersed into the strong acid solution (pH 1), the static contact angle is gradually decreased with the increment of immersing time. After immersing for 24 h, the static contact angle is decreased to 140°, which turns to a general hydrophobic surface from superhydrophobic one. The reason may be ascribed to the instability of the modifier of 1H,1H,2H,2H-perfluorodecyltrichlorosilane in the strong acid solution. Actually, the superhydrophobic performances mainly depend on two aspects: lotus leaf-like hierarchical micro/nanostructure and the modifier. Undoubtedly, the fabricated solid substrate will be not easily broken. Accordingly, its anticorrosion derived from superhydrophobic stability will be definitely improved to realize its real application as an engineering material in strong acid and base solutions when the fabricated surface has been modified by some strong acid-/base-proof organic substances with a low free energy.

Besides the above-mentioned functions, interestingly, the fabricated superhydrophobic surface can also be employed as concentrators avoiding the diffusion of solution containing analytes. With the water droplet on its surface gradually evaporated, the volume of droplet would be contracted, leading to the decrease in its diameter, which is agreement with previous reports.[45,46] As shown in Figure 10a, the morphology evolution for the water droplet of 10 μL is presented. Clearly, with the evaporating time increase to 40 min, the contacting baseline between water droplet and surface gradually decreases. After about 60 min, the water droplet is continuously and completely evaporated with an unchanged baseline, which can be seen from the states at the evaporating time of 60 and 75 min. On the basis this phenomenon, the fabricated superhydrophobic surface can be used as concentrators and further employed as an example to improve the sensitivity in the SERS detection and analysis. In Figure 10b, the schematic evaporation process of a droplet containing Au nanoparticles and CV has been presented. Inferred from the morphology evolution shown Figure 10a, it can be concluded that the concentration of Au nanoparticles and CV will gradually increase with the evaporation of water. When the water is completely evaporated, the Au nanoparticles and CV contracted a small point, which is shown in Figure S6b in the Supporting Information. It is different from that of the water droplet containing Au nanoparticles and CV on the glass slide. As described in Figure S6a in the Supporting Information, the droplet will rapidly spread and diffuse on the glass surface. Finally, a larger circle area of the dried Au nanoparticles and CV is formed, which is about 100 time of that on the superhydrophobic surface. Accordingly, Au nanoparticles and CV per area on glass slide is much less than that on the superhydrophobic surface. Combined with the SERS measurement, the Raman intensity of CV at a random selected point on the superhydrophobic surface is much stronger that on glass

slide, as shown in Figure 10c. To truly evaluate the enhanced effect, we performed the SERS signal mapping of a line scan on both substrates. Here, a strong peak at 1616 cm^{-1} is selected only to make a comparison between two substrates, which is shown in Figure 10d. Compared with that on the superhydrophobic surface, the signal is very weak and neglected on the glass slide except the edge of the dried circle, which is well in agreement with that shown in Figure 10c. Interestingly, on the superhydrophobic surface the peak intensity presents a periodic change along the protrusion-like microstructure following the green line in Figure 10d, which is ascribed to the periodic distribution of microprotrusions on the substrate. Compared with a glass slide, the intensity of SERS signal is enhanced more than 10−100 times. Obviously the superhydrophobic surface will effectively concentrate the analyte and improve its determination.[47] Through employing the SERS detection as an example, the fabricated superhydrophobic surface with heterohierarchical micro/nanostructure presents a great perspective in the field of analysis.

CONCLUSIONS

Heterohierarchical micro/nanostructure tetragonal array consisted of engineering materials of microprotrusion-like Cu and secondary nanostructure of dendrite Ag have been fabricated via a primary cell-induced deposition and a facile galvanic displacement reaction combined with a photolithography approach on the Cu substrate. Through adjusting the space-confined deposition and displacement reaction time, the morphology of microprotrusion-like Cu and dendritic Ag nanostructure could be finely manipulated, which leads to the tunable wettability. For the fabricated surface with regular heterohierarchical micro/nanostructure array, it presents a remarkable superhydrophobic performance with a contact angle of 165° and a sliding angle of less than 2° for a 5 μL water droplet after the surface fluoration. Furthermore, the fabricated superhydrophobic surfaces show an excellent self-cleaning performance and a good stability in a wide pH range, that is, not only for pure water but also for corrosive liquids including acidic, basic, and NaCl aqueous solutions. Finally, the fabricated surface has been potentially used as concentrators avoiding the diffusion of solution containing analytes to improve the SERS detection. Compared with a glass slide, the intensity of SERS signal is enhanced more than 10−100 times, which presents a great perspective concerning to the detection and analysis of the diluted analytes.

ASSOCIATED CONTENT

Supporting Information

Effects of the deposition time on the diameter of microprotrusion-like Cu (Figure S1). SEM images and static contact angles of the Cu foil uncovered with photoresist after primary cell-induced deposition and following galvanic displacement reaction (Figure S2). Typical SEM images of the fabricated surface with microprotrusion and hetero/hierarchical micro/nanostructure and their static contact angle and dynamic contact angle plots (Figure S3). Contact time of a bouncing drop as a function of impact velocity and drop radius (Figure S4). The static contact angles under strong acid solution, strong base solution, and NaCl aqueous solution (Figure S5). Photos of the solution containing Au nanoparticles and CV before and after drying (Figure S6). This material is available free of charge via the Internet at http://pubs.acs.org/.

AUTHOR INFORMATION

Corresponding Author

*E-mail: xingjiuhuang@iim.ac.cn. Tel.: +86-551-5591142. Fax: +86-551-5592420.

Notes

The authors declare no competing financial interest.

ACKNOWLEDGMENTS

This work was supported by the National Key Scientific Program-Nanoscience and Nanotechnology (2011CB933700), and National Natural Science Foundation of China (21073197). X.J.H. acknowledges the CAS Institute of Physical Science, University of Science and Technology of China (2012FXCX008), for financial support.

REFERENCES

(1) Sun, T. L.; Feng, L.; Gao, X. F.; Jiang, L. *Acc. Chem. Res.* **2005**, *38*, 644−652.
(2) Li, X. M.; Reinhoudt, D.; Crego-Calama, M. *Chem. Soc. Rev.* **2007**, *36*, 1350−1368.
(3) Ren, H. X.; Chen, X.; Huang, X. J.; Im, M.; Kim, D. H.; Lee, J. H.; Yoon, J. B.; Gu, N.; Liu, J. H.; Choi, Y. K. *Lab Chip* **2009**, *9*, 2140−2144.
(4) Li, H. L.; Wang, J. X.; Yang, L. M.; Song, Y. L. *Adv. Funct. Mater.* **2008**, *18*, 3258−3264.
(5) Zhu, Y.; Zhang, J. C.; Zheng, Y. M.; Huang, Z. B.; Feng, L.; Jiang, L. *Adv. Funct. Mater.* **2006**, *16*, 568−574.
(6) Shiu, J. Y.; Chen, P. *Adv. Funct. Mater.* **2007**, *17*, 2680−2686.
(7) Shirtcliffe, N. J.; McHale, G.; Newton, M. I.; Zhang, Y. *ACS Appl. Mater. Interfaces* **2009**, *1*, 1316−1323.
(8) Cheng, Y. T.; Rodak, D. E.; Wong, C. A.; Hayden, C. A. *Nanotechnology* **2006**, *17*, 1359−1362.
(9) Bittoun, E.; Marmur, A. *Langmuir* **2012**, *28*, 13933−13942.
(10) Patankar, N. A. *Langmuir* **2004**, *20*, 8209−8213.
(11) Roach, P.; Shirtcliffe, N. J.; Newton, M. I. *Soft Matter* **2008**, *4*, 224−240.
(12) Jonas, U.; Vamvakaki, M. *Angew. Chem., Int. Ed.* **2010**, *49*, 4542−4543.
(13) Lee, E. J.; Kim, J. J.; Cho, S. O. *Langmuir* **2010**, *26*, 3024−3030.
(14) Nakanishi, T.; Michinobu, T.; Yoshida, K.; Shirahata, N.; Ariga, K.; Moehwald, H.; Kurth, D. G. *Adv. Mater.* **2008**, *20*, 443−446.
(15) Wang, S. T.; Song, Y. L.; Jiang, L. *Nanotechnology* **2007**, *18*, 015103−015105.
(16) Xue, Y. H.; Chu, S. G.; Lv, P. Y.; Duan, H. L. *Langmuir* **2012**, *28*, 9440−9450.
(17) Xu, W. G.; Liu, H. Q.; Lu, S. X.; Xi, J. M.; Wang, Y. B. *Langmuir* **2008**, *24*, 10895−10900.
(18) Feng, J. S.; Tuominen, M. T.; Rothstein, J. P. *Adv. Funct. Mater.* **2011**, *21*, 3715−3722.
(19) Lee, Y. W.; Park, S. H.; Kim, K. B.; Lee, J. K. *Adv. Mater.* **2007**, *19*, 2330−2335.
(20) Wang, M. F.; Raghunathan, N.; Ziaie, B. *Langmuir* **2007**, *23*, 2300−2303.
(21) Guo, Z.; Chen, X.; Li, J.; Liu, J. H.; Huang, X. J. *Langmuir* **2011**, *27*, 6193−6200.
(22) Liu, K. S.; Jiang, L. *Nanoscale* **2011**, *3*, 825−838.
(23) Liu, L. J.; Xu, F. Y.; Ma, L. *J. Phys. Chem. C* **2012**, *116*, 18722−18727.
(24) Xu, X. H.; Zhang, Z. Z.; Yang, J. *Langmuir* **2010**, *26*, 3654−3658.
(25) Ye, W. C.; Yan, J. F.; Ye, Q. A.; Zhou, F. *J. Phys. Chem. C* **2010**, *114*, 15617−15624.
(26) Li, L.; Breedveld, V.; Hess, D. W. *ACS Appl. Mater. Interfaces* **2012**, *4*, 4549−4556.
(27) Wang, G. Y.; Zhang, T. Y. *ACS Appl. Mater. Interfaces* **2012**, *4*, 273−279.
(28) Qian, B. T.; Shen, Z. Q. *Langmuir* **2005**, *21*, 9007−9009.

(29) Guo, Z. G.; Zhou, F.; Hao, J. C.; Liu, W. M. *J. Am. Chem. Soc.* **2005**, *127*, 15670−15671.
(30) Ishizaki, T.; Sakamoto, M. *Langmuir* **2011**, *27*, 2375−2381.
(31) Lin, P.; Lin, C. W.; Mansour, R.; Gu, F. *Biosens. Bioelectron.* **2013**, *47*, 451−460.
(32) Lai, Y.; Pan, F.; Xu, C.; Fuchs, H.; Chi, L. *Adv. Mater.* **2013**, *25*, 1682−1686.
(33) Huang, X. J.; Lee, J. H.; Lee, J. W.; Yoon, J. B.; Choi, Y. K. *Small* **2008**, *4*, 211−216.
(34) Huang, X. J.; Kim, D. H.; Im, M.; Lee, J. H.; Yoon, J. B.; Choi, Y. K. *Small* **2009**, *5*, 90−94.
(35) Yeh, K. Y.; Cho, K. H.; Chen, L. J. *Langmuir* **2009**, *25*, 14187−14194.
(36) Cortese, B.; D'Amone, S.; Manca, M.; Viola, I.; Cingolani, R.; Gigli, G. *Langmuir* **2008**, *24*, 2712−2718.
(37) Shirtcliffe, N. J.; McHale, G.; Newton, M. I.; Chabrol, G.; Perry, C. C. *Adv. Mater.* **2004**, *16*, 1929−1932.
(38) Li, Z. B.; Meng, G. W.; Huang, Q.; Zhu, C. H.; Zhang, Z.; Li, X. D. *Chem.—Eur. J.* **2012**, *18*, 14948−14953.
(39) Yi, Z.; Tan, X. L.; Niu, G.; Xu, X. B.; Li, X. B.; Ye, X.; Luo, J. S.; Luo, B. C.; Wu, W. D.; Tang, Y. J.; Yi, Y. G. *Appl. Surf. Sci.* **2012**, *258*, 5429−5437.
(40) Chen, X.; Cui, C. H.; Guo, Z.; Liu, J. H.; Huang, X. J.; Yu, S. H. *Small* **2011**, *7*, 858−863.
(41) Guo, Z. G.; Liu, W. M.; Su, B. L. *Appl. Phys. Lett.* **2008**, *92*, 063104−063106.
(42) Lai, Y. K.; Tang, Y. X.; Huang, J. Y.; Wang, H.; Li, H. Q.; Gong, D. G.; Ji, X. B.; Gong, J. J.; Lin, C. J.; Sun, L.; Chen, Z. *Soft Matter* **2011**, *7*, 6313−6319.
(43) Wang, C. F.; Wang, Y. T.; Tung, P. H.; Kuo, S. W.; Lin, C. H.; Sheen, Y. C.; Chang, F. C. *Langmuir* **2006**, *22*, 8289−8292.
(44) Xi, J. M.; Feng, L.; Jiang, L. *Appl. Phys. Lett.* **2008**, *92*, 053102−053104.
(45) Lu, L. Q.; Zheng, Y.; Qu, W. G.; Yu, H. Q.; Xu, A. W. *J. Mater. Chem.* **2012**, *22*, 20986−20990.
(46) De Angelis, F.; Gentile, F.; Mecarini, F.; Das, G.; Moretti, M.; Candeloro, P.; Coluccio, M. L.; Cojoc, G.; Accardo, A.; Liberale, C.; Zaccaria, R. P.; Perozziello, G.; Tirinato, L.; Toma, A.; Cuda, G.; Cingolani, R.; Di Fabrizio, E. *Nat. Photonics* **2011**, *5*, 683−688.
(47) Xu, F. G.; Zhang, Y.; Sun, Y. J.; Shi, Y.; Wen, Z. W.; Li, Z. *J. Phys. Chem. C* **2011**, *115*, 9977−9983.